Journal of Magnetism and Magnetic Materials 403 (2016) 172–180

Contents lists available at ScienceDirect

Journal of Magnetism and Magnetic Materials

journal homepage: www.elsevier.com/locate/jmmm

# Energetics and the magnetic state of $Mn_2$ adsorbed on Au(111): Dimer bond distance dependence

S. López-Moreno [a,*], J. Mejía-López [b,c], Francisco Munoz [c,d], A. Calles [e], J.L. Morán-López [f]

[a] CONACYT Research Fellow - Centre for Corrosion Research, Autonomous University of Campeche, Av. Héroe de Nacozari 480, Campeche 24070, Mexico
[b] Facultad de Física, Centro de Investigación en Nanotecnología y Materiales Avanzados CIEN-UC, Pontificia Universidad Católica de Chile, Santiago, Chile
[c] Centro para el Desarrollo de la Nanociencia y la Nanotecnología CEDENNA, Avda. Ecuador 3493, Santiago, Chile
[d] Departamento de Física, Facultad de Ciencias, Universidad de Chile, Casilla 653, Santiago, Chile
[e] Facultad de Ciencias, Universidad Nacional Autónoma de México, Apdo. Post. 70-646, México D. F. 04510, Mexico
[f] Advanced Materials Department, IPICYT, Camino a la Presa de San José 2055, 78216, San Luis Potosí, San Luis Potosí, Mexico

ARTICLE INFO

*Article history:*
Received 24 October 2014
Received in revised form
19 November 2015
Accepted 26 November 2015
Available online 2 December 2015

*Keywords:*
Supported manganese dimer
Magnetic bi-stability
Diffusion of $Mn_2$

ABSTRACT

In this work we present a theoretical study of the adsorption $Mn_2$ dimer on the Au(111) surface. Here we use the density functional theory to construct a map of adsorption energies, $E_A$, of $Mn_2$ on a Au(111) surface as a function of interatomic bond distance, $d_{Mn-Mn}$, among Mn atoms. We employed a $4\times4$ supercell of Au(111) surface which lead us to reach $d_{Mn-Mn}$ values in the range from 2.6 to 6.8 Å. To make a full study of the adsorption energies we considered the antiferromagnetic (AFM) and ferromagnetic (FM) states of the $Mn_2$ on the surface. The energy landscape contains local minima when the Mn atoms are adsorbed above triangular sites and barriers that the Mn adatoms have to overcome when they move across the Au(111) surface along various paths. Our results show that the lowest energy state corresponds to the state in which the Mn atoms are next-nearest neighbors and are antiferromagnetically coupled. Furthermore, all the local minima with higher bonding energy are also those in the antiferromagnetic state. Nevertheless we find a short interval in which the FM state has lower energy than the AFM one. Finally, scanning tunneling microscope simulations for various dimer configurations on surface are reported.



## 1. Introduction

Manganese is one of the most attractive elements of the transition metal series, but also the most elusive to understand [1–3]. It is the transition metal with the highest atomic moment ($5\ \mu_B$), zero orbital moment, and the high energy between *d*and *s*-states makes the $3d^54s^2$ atomic configuration particularly stable [4]. The outer *s*-shell is fully occupied but the *d* shell is only half-filled. Furthermore, the unfilled *d*-subshell lies 2.14 eV above the occupied and the atomic moment is resilient to minor changes; this is the reason why dilute Mn atoms in semiconductors and as a main component in the ternary Heusler alloys [5,6] keep a high magnetic moment.

The bonding in the Mn dimer is weak, and is cataloged as a Van der Walls molecule. This feature hinders the experimental study in the gas phase, but reports of high-temperature mass spectroscopy [7,8] assign its binding energy values that range from 0.02 to 0.55 eV. Another estimate obtained from the photodissociation [9] amounts to 0.6 eV.

In relation to the dimer magnetic properties, various experimental techniques, like electron spin resonance [10], circular magnetic dichroism [11], absorption fluorescence [12], and resonance Raman spectroscopy [13], indicate an antiferromagnetic coupling with total spin $S=0$. This last estimation corresponds to $Mn_2$ deposited in rare-earth matrixes.

On the other hand, the free manganese dimer has been studied theoretically in detail, using various models and theories, and it is still a field of debate. A state of the art *ab initio* calculation and comparison with other results is reported by Buchachenko et al. [14]. A very interesting result by Mejía-López et al. based on a density functional theory study shows that the magnetic coupling depends on the distance between the two atoms [2]; the ferromagnetic (FM) and antiferromagnetic (AFM) states are stable above and below 3.06 Å, respectively.

Since most of the nanoscale technological applications requires the deposition of magnetic atoms, small clusters or thin films on particular substrates, in the last decade there have been many attempts to stabilize Mn atoms in metallic substrates, expecting to find appropriate conditions such that the Mn interaction, mediated by the surface electrons, produce a ferromagnetic coupled

* Corresponding author.
*E-mail address:* sinlopez@uacam.mx (S. López-Moreno).

http://dx.doi.org/10.1016/j.jmmm.2015.11.079
0304-8853/

system.

For example, the growth of Mn on Au(111) surfaces has been studied by means of scanning tunneling microscopy and low energy electron diffraction [15]. They found that the growth of Mn as a function of coverage evolves in the following manner: for submonolayer coverages the Mn atoms nucleate at the elbows of the $(22 \times \sqrt{3})$ reconstructed Au(111) surface and partially occupy subsurface sites, forming an incipient surface alloy. For larger coverages the Mn atoms accumulate to form two dimensional alloy islands. This kind of growth continues up to 6 ML, coverage that produces a Mn thin film. Unfortunately the magnetic properties were not measured.

Manganese deposited on copper (100) [16], and (110) [17], and silver (110) [18] surfaces have been also reported. They find ordered alloys at half-monolayer coverage with the Mn atoms located in hollow surface central sites. From the magnetic measurements, they conclude that the Mn atoms conserve a reduced magnetic moment, due to the electron hybridization with the metallic surface atoms. Furthermore, they also conclude that the magnetic coupling is antiferromagnetic. Very recently an experimental/theoretical study of $Mn_2$ on Ag (111) showed a virtually degenerated $Mn_2$ groundstate, but the attachment of H to the dimer leads to marked changes in the dimer electronic and magnetic structure [19].

With the aim to understand the monoatomic and dimer Mn adsorption on the Au(111) we calculated, within the framework of the density functional theory, and reported in recent papers [20,21] the chemisorption geometry, the binding energy, and the magnetic moments through selfconsistent calculations of the electronic structure. By considering ferro and antiferro-arrangements we found that the Mn atoms chemisorb on three-coordinated hollow sites with antiferromagnetic coupling. The geometries considered were only when the Mn are nearest and next nearest neighbors.

To contribute further to the understanding of this phenomenon, in this paper we report a first principles study of the adsorption energy and the magnetic state of the Mn-dimer adsorbed on the Au(111) surface as a function of the interatomic bond distance among the Mn atoms on the surface. The main goals of this paper are (i) to identify the lowest state energy of the $Mn_2$/Au(111) system as a function of the interatomic bond distance, $d_{Mn-Mn}$, by considering the FM and AFM coupling among Mn atoms on the surface; (ii) to study the energy barriers when the Mn atoms that form the $Mn_2$ dimer move across the surface for $d_{Mn-Mn}$ values in a range from $\approx 2.5$ to 6.8 Å. We present the energetic landscape that produce the $Mn_2$ adsorption, (iii) to quantify the deformations on the Au-triangles that host the Mn atoms, (iv) to study the of the Au(111) Schockley state in the magnetic interactions, and (v) to calculate some STM images of the $Mn_2$ configurations.

## 2. Computational methods

Calculations of the total energy were performed within the framework of the density functional theory (DFT) and the projector-augmented wave (PAW) [22,23] method, as implemented in the Vienna *ab initio* simulation package (VASP) [24–27]. The exchange and correlation energy was described within the generalized gradient approximation (GGA) in the Perdew–Burke–Ernzerhof (PBE) [28] prescription. We used a plane-wave energy cutoff of 290 eV and have carefully checked the convergence of our calculations. This assure that in the relaxed equilibrium configuration the forces are less than 0.01 eV/Å.

As a first step we calculated the ground state of bulk gold. As is well known, Au crystallizes in the $Fm\bar{3}m$ structure, for which we found the lattice parameter $a = 4.166$ Å, in good agreement with previous theoretical calculations and experimental results [20,21,29]. The Au(111) surface structure was built with this value of $a$. We modeled the surface region as a slab of five layers; two of them were kept fixed to the bulk values and the other three were allowed to relax. The Au(111) surface presents a well-known $23 \times \sqrt{3}$ herringbone reconstruction, provided the large size of the reconstructed supercell, and our interest on the low Mn coverage it is a reasonable approximation just to ignore this reconstruction. Furthermore, a recent study has validated this approximation [30].

After the structural relaxation of the three topmost layers we found that the surface layer expands 1.6%, and the second one compresses 0.2%, these values compare well with experimental data [31]. Due to the periodic conditions in the calculations, to simulate the vacuum zone we have considered a distance of 12 Å (equivalent to five surface layers). According to our previous work, the surface energy changes by less than 0.2% when the vacuum thickness is increased to 14 Å [20]. Therefore, we can disregard spurious self-interactions.

To simulate the monomer and dimer Mn adsorption, we employed a $4 \times 4$ supercell with a thickness of 5 layers with 16 atoms per layer, representing a coverage of $\frac{1}{16}$ and $\frac{1}{8}$ ML for Mn and $Mn_2$ adsorbed on the surface, respectively. Monkhorst–Pack scheme was employed to discretize the Brillouin-zone (BZ) integrations [32] with a set of 14 special $k$-points in the irreducible two-dimensional BZ.

For the optimized structure of Au(111) slab we have calculated the surface energy by:

$$E_s = \frac{E_{\text{semi-inf}} - NE_{\text{bulk}}}{2N}, \tag{1}$$

where $E_{\text{semi-inf}}$, $E_{\text{bulk}}$, and $N$ are the energy of clean surface, the energy of Au in the bulk per atom, and the number of surface atoms involved, respectively. We obtain a value for surface energy of 0.065 eV, which is in good agreement with the values reported in the literature [20,33–35] which range from 0.044 to 0.055 eV. The strong spin–orbit coupling of gold yields a sizable Rashba effect on the gold surface bands, but its influence in the adsorption of Mn is rather small, as was pointed in our previous report [20]. Since our interest is the adsorption energy and their respective geometries, the use of a scalar-relativistic pseudopotential is enough, and we can ignore vector-relativistic effects.

We calculated the adsorption energy, $E_A$, as follows:

$$E_A = \frac{E_{\text{Total}} - E_{\text{semi-inf}} - \mathcal{N}E_{\text{Mn}}}{\mathcal{N}}, \tag{2}$$

where $E_{\text{Total}}$, $E_{\text{semi-inf}}$, $E_{\text{Mn}}$, and $\mathcal{N}$ are the total energy of the slab plus Mn atoms adsorbed on the surface, the energy of the clean surface, the energy of an isolated Mn atom, and the number of Mn atoms adsorbed on the surface, respectively.

## 3. Results and discussion

Previous theoretical studies [20,21] have demonstrated that Mn atoms can be adsorbed on four different sites over the Au(111) surface: on top of a surface Au atom, on the bridge position between two surface Au atoms, and in two different threefold hollow sites. The threefold coordinated sites are of two types, one that follows the hcp sequence, and other that follows the fcc stacking order. It was observed that Mn atoms adsorbed on the first one (top site) have the weakest bond energy among the four sites. Also, the results show that Mn atoms adsorbs strongly in the threefold coordinated sites of Au(111) surface, whereas the Mn atoms adsorbed on a bridge site are $\approx 70$ meV weaker in energy than in the threefold coordinated sites. Therefore, we limit our study to the

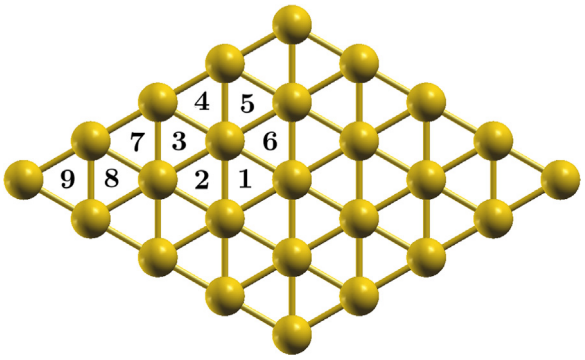


**Fig. 1.** Considered adsorption sites on $4\times4$ Au(111) surface. The sites 2, 4, 6, 7, and 9 are hcp (ABA stacking) whereas 1, 3, 5, and 8 are fcc (ABC stacking).

adsorption of Mn atoms in hcp and fcc sites. We found that the adsorption energy, $E_A$, of Mn in an fcc site is just $\approx 10$ meV stronger in energy than in the hcp one, in good agreement with previous results [20]. This small difference in the $E_A$ between hcp and fcc sites has also been observed in other transition metal surfaces such as Pt, Ir, Cu, and Ni [36].

### 3.1. Adsorption energy and magnetic state

The next step is to make a map of the adsorption energy of the $Mn_2$ dimer at the Au(111) surface as a function of the interatomic bond distance among the two Mn atoms, $d_{Mn-Mn}$. We only consider the case of the dimer lying parallel to the surface. Thus, to observe the effect of $d_{Mn-Mn}$ in the value of the adsorption energy we have positioned the two Mn atoms on different sites at the surface. According to Fig. 1, the considered sites where the two Mn atoms are adsorbed in increasing order of $d_{Mn-Mn}$ are 1–2, 1–3, 1–4, 1–7, 1–8, 5–8, 6–8, and 1–9. The site labeled with number 1 is of fcc type. Then, after locating the second Mn atom at other of the various sites we allow the system to relax the internal coordinates.

The adsorption energies, $E_A$, of Mn atoms in the different sites studied according to Fig. 1, the magnetic moment of each Mn atom, $\mu$, and the value of $d_{Mn-Mn}$, for FM and AFM configurations are listed in Tables 1 and 2. In Table 1 we report the results for the case in which we fix one Mn atom in site 1 and the second Mn atom is located following the sequence $2\rightarrow3\rightarrow7\rightarrow8\rightarrow9$, and Table 2 corresponds to the situation in which one Mn atom is at site 5 and the second in the sites $4\rightarrow3\rightarrow7\rightarrow8$. As a general trend, we observed that the lowest energy state for all the studied geometries corresponds to those in which the Mn magnetic moments are coupled antiferromagnetically, and the most stable state

**Table 1**
$Mn_2$ adsorption data as a function of Mn–Mn bond distance $d_{Mn-Mn}$. One of the Mn atoms is kept fixed on site 1 and the other moves from site 2 to 9 following the sequence $2\rightarrow3\rightarrow7\rightarrow8\rightarrow9$ (see Fig. 1), on the $4\times4$ Au(111) surface with an atomic coverage of $\frac{1}{8}$ ML. Here, $E_A$ is the adsorption energy, $\mu$ is the magnetic moment per Mn atom, and $d_{Mn-Mn}$ is the Mn–Mn interatomic bond distance. We considered both the ferromagnetic (FM) and antiferromagnetic (AFM) configurations.

| Site | $E_A$ (eV) | | $\mu$ ($\mu_B$) | | | | $d_{Mn-Mn}$ (Å) | |
|---|---|---|---|---|---|---|---|---|
| | FM | AFM | FM | | AFM | | FM | AFM |
| 1-2 | −5.316 | −5.368 | 4.16 | 4.15 | 4.18 | −4.17 | 2.699 | 2.573 |
| 1-3 | −5.440 | −5.504 | 4.19 | 4.19 | 4.22 | −4.22 | 2.896 | 2.765 |
| 1-4 | −5.344 | −5.382 | 4.26 | 4.27 | 4.26 | −4.26 | 3.522 | 2.915 |
| 1-7 | −5.306 | −5.316 | 4.29 | 4.28 | 4.30 | −4.29 | 4.510 | 4.508 |
| 1-8 | −5.328 | −5.342 | 4.29 | 4.29 | 4.29 | −4.29 | 5.105 | 5.116 |
| 1-9 | −5.332 | −5.342 | 4.30 | 4.30 | 4.30 | −4.29 | 6.803 | 6.803 |

**Table 2**
$Mn_2$ adsorption data as a function of Mn–Mn bond distance $d_{Mn-Mn}$. One of the Mn atoms is kept fixed on site 5 and the other moves from site 4 to 8 following the sequence $4\rightarrow3\rightarrow7\rightarrow8$ (see Fig. 1), on the $4\times4$ Au(111) surface with an atomic coverage of $\frac{1}{8}$ ML. Here, $E_A$ is the adsorption energy, $\mu$ is the magnetic moment per Mn atom, and $d_{Mn-Mn}$ is the Mn–Mn interatomic bond distance. We considered both the ferromagnetic (FM) and antiferromagnetic (AFM) configurations.

| Site | $E_A$ (eV) | | $\mu$ ($\mu_B$) | | | | $d_{Mn-Mn}$ (Å) | |
|---|---|---|---|---|---|---|---|---|
| | FM | AFM | FM | | AFM | | FM | AFM |
| 5–4 | −5.316 | −5.368 | 4.16 | 4.15 | 4.18 | −4.17 | 2.699 | 2.573 |
| 5–3 | −5.440 | −5.504 | 4.19 | 4.19 | 4.22 | −4.22 | 2.896 | 2.765 |
| 5–7 | −5.306 | −5.316 | 4.29 | 4.28 | 4.30 | −4.29 | 4.510 | 4.508 |
| 5–8 | −5.302 | −5.308 | 4.29 | 4.29 | 4.30 | −4.30 | 5.892 | 5.892 |

corresponds to the situation in which the two Mn atoms are adsorbed in fcc triangular lattice points (1–3). This configuration is more stable than (1–2), where two adatoms occupy neighbor surface sites. Furthermore, as we discuss in the next paragraphs the (1–2) configuration is metastable. Other two clear relative minima are the configurations (1–8) and (1–9), with very similar values.

The results also show that AFM and FM states have similar Mn–Mn interatomic bond distances when the atoms are adsorbed at fixed threefold hollow sites for values of $d_{Mn-Mn} > 4.5$ Å. For shorter distances we observed that the interatomic bond distance Mn–Mn for AFM configurations are shorter than for the FM one; the main difference occurs in the 1–4 configuration. These results show that the magnetic coupling among Mn atoms is stronger for values of $d_{Mn-Mn} < 4.5$ Å. With respect to the magnetic moment of Mn atoms we found that there are only small differences between the FM and AFM states, and we can see from Tables 1 and 2 that $\mu$ increases proportionally to $d_{Mn-Mn}$. The values range from 4.16 to 4.3 $\mu_B$. We can also notice that small differences in the magnitude of the magnetic moments are produced by the different fcc and hcp environments.

To illustrate better our results, we have plotted in Fig. 2 the adsorption energy as a function of the interatomic bond distance $d_{Mn-Mn}$. The upper (lower) panel corresponds to the sequence in which one of the Mn atoms is located in site 1 and the other is in $2\rightarrow3\rightarrow7\rightarrow8\rightarrow9$ ($4\rightarrow3\rightarrow7\rightarrow8$). Here, the dashed lines correspond for the FM configuration of the magnetic moments and the continuous line to the AFM one. According to this figure and the data of $d_{Mn-Mn}$ from Table 1, we see there is a crossing in the state of lowest energy from the AFM to the FM one as one goes from the configuration 1–3 site to 1–4. Also, there is a second crossing to the AFM state when one goes from the 1–4 to 1–7 state. After $d_{Mn-Mn} = 4.508$ Å the lower energy state corresponds to the AFM alignment. Thus, it is important to know the behavior of the adsorption energy in the intermediate positions between the fixed sites of Fig. 2; in particular in the range of bond lengths where the change from AFM to FM occurs and vice-versa.

### 3.2. The adsorption energy landscape

In order to study the detail of the energy barriers for the intermediate distances between the relative minima, we have used the nudge elastic band (NEB) method [37,38], which in addition will help us to calculate the dissociation paths and diffusion barriers for the Mn dimer on the Au(111) surface. The NEB method is used to find saddle points and minimum energy paths between known reactants and products. The method works by optimizing a number of intermediate images (i.e. positions or states) along a reaction path. Each image finds the lowest energy of possible configuration while maintaining equal spacing with neighboring

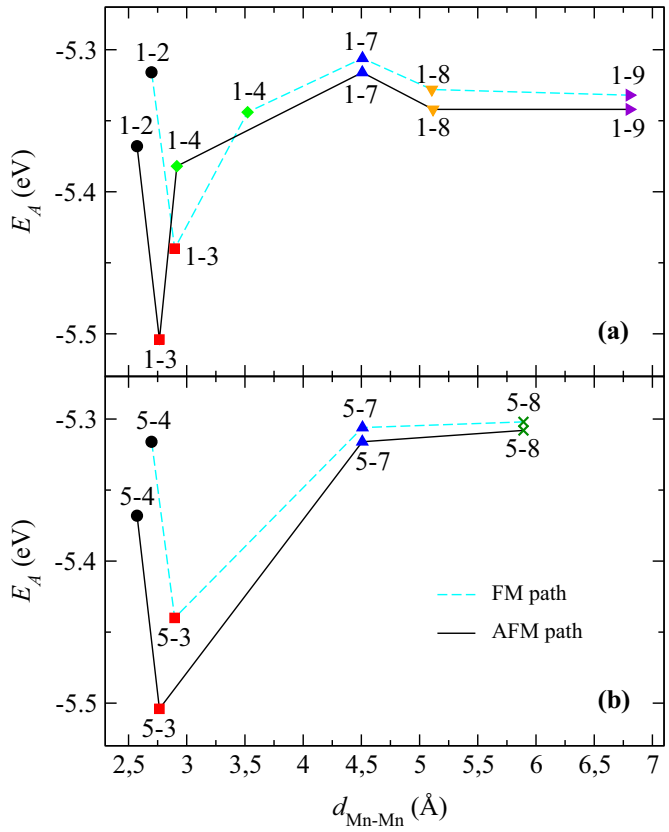


**Fig. 2.** (a) Adsorption energy $E_A$ as a function of the interatomic bond distance among Mn atoms on the $4 \times 4$ Au(111) surface. In the upper (lower) panel, the numbers 1–2, 1–3, 1–4, 1–7, 1–8, 5–8, 6–8, and 1–9 (5–4, 5–3, 5–7 and 5–8) refer to the sites where Mn atoms are adsorbed, see Fig. 1.

images. The reaction paths were determined in a series of separated calculations: from 1–2 to 1–3, 1–3 to 1–7, 1–7 to 1–8, 1–8 to 1–9, and completed the calculation with the path from 1–3 to 1–4, for the AFM and FM magnetic moment configurations.

The reaction paths of the minimum adsorption energy of Mn atoms on the Au(111) surface are shown in Fig. 3. The fixed states from Table 1 appear as blue triangles, while the intermediate states calculated with the NEB method are denoted by black circles and green squares for AFM paths, whereas the FM ones are denoted by cyan stars and orange diamonds. The fitting of the respective intermediate and fixed states are represented by continuous and dashed lines, respectively. According to the AFM path of Fig. 3(a), the configuration 1–2 is metastable and the second atoms could tend to move to the minimum of position 3. Furthermore, to move the Mn atom from site 3 to 4 or 7 it is necessary an energy of 122 and 188 meV. For more distant sites the energies get reduced to 63 meV $(7 \rightarrow 8)$ and 51 meV $(8 \rightarrow 9)$. Similar amounts of energy are needed when one considers the ferromagnetic arrangement. The reaction path to move a Mn atom from position 3 to 4 is shown in Fig. 3(b). The energy barriers we found are in agreement with the experimental results of Fonin et al., they reported the formation of small and isolated Mn islands [15] for a coverage of $\theta = 0.01$. Which is consistent with a minimum of energy for nearest neighbors, but with a maximum for intermediate regions.

### 3.3. Geometrical surface deformation produced by the Mn adsorption

In Fig. 4 we show the deformation that the Au-surface triangles suffer upon the chemisorption process as a function of the Mn–Mn bond distance. In the *y*-axis we plot the relative area deformation in the presence of the two Mn atoms, defined as follows

$$A_{n,rel} = \frac{A_n - A_{clean}}{A_{clean}} \cdot 100\%, \tag{3}$$

where $A_n$ is the area of the deformed triangle in the presence of the Mn atoms and $A_{clean}$ the non-perturbed clean Au surface triangle (3.758 Å$^2$). The *x*-axis is the Mn–Mn bond distance, $d_{\text{Mn–Mn}}$.

We present the results for the antiferromagnetic arrangements and for the areas of the sites labeled as 1, 2, 3, 7, 8 and 9. We recall the fact that one of the atoms is always sitting in site 1. Thus, for example, the results for the geometry 1–2 show that the triangles 1, 2 and 3 suffer an expansion, being the distortion of triangle 2 the largest. The other three triangles, 7, 8 and 9, get compressed. As the second Mn atom moves from site 2 to 9 the change in area for each triangle goes through minima and maxima. However, it is important to notice that the deformation of the triangles where

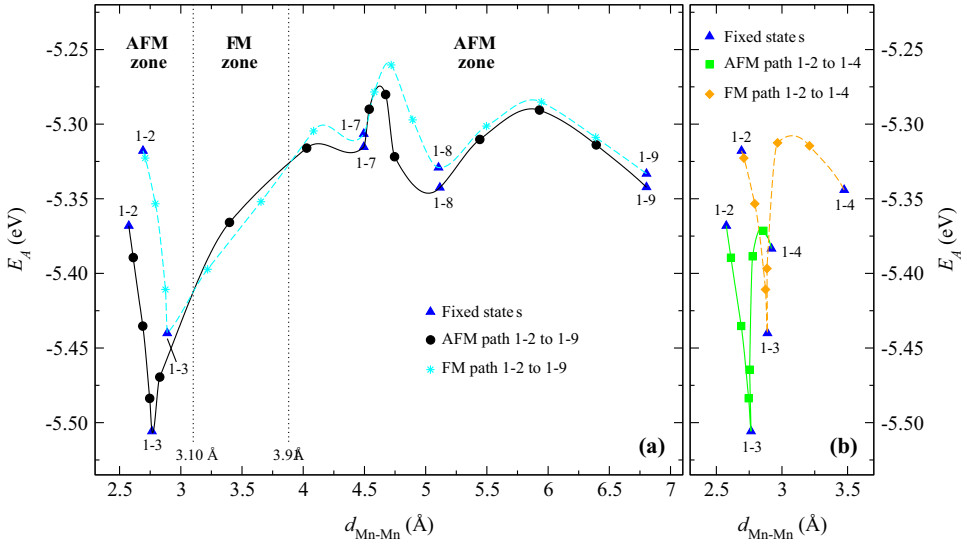


**Fig. 3.** Reaction paths (a) 1–2 to 1–9 and (b) 1–2 to 1–4 for interaction of Mn atoms in Au(111) surface, where **FM** and **AFM** are for ferromagnetic and antiferromagnetic, respectively. The continuous and dashed lines are interpolations from the calculated points and are given only as a guide to the eye. The corresponding adsorption energy and interatomic bond distances for 1–2, 1–3, 1–4, 1–7, 1–8, and 1–9 fixed sites are listed in Table 1. (For interpretation of the references to color in the text, the reader is referred to the web version of this paper.)

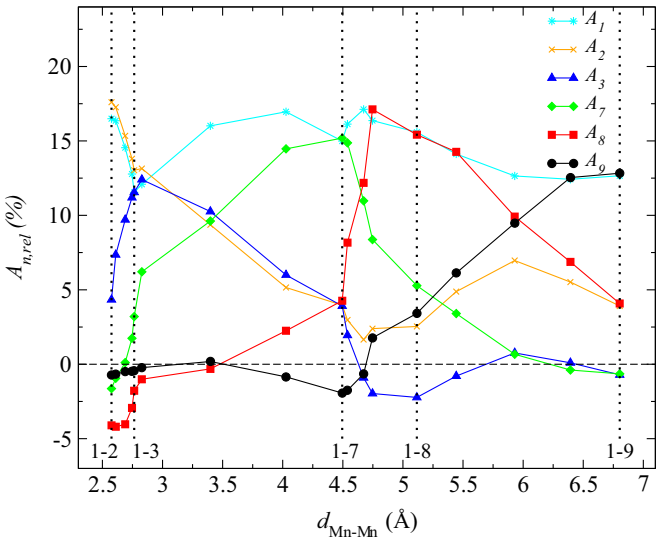


**Fig. 4.** Variation of the triangle area for the most representative threefold hollow sites of Fig. 1 relative to the area of the threefold hollow site of clean surface as function of the Mn–Mn interatomic bond distance.

the Mn atoms are located have equal or similar values, if the two sites are fcc–fcc or fcc–hcp. This difference gets negligible when $d_{Mn-Mn}$ is larger than 4.5 Å. Furthermore, one notices that for the case 1–9 the expansion of the 1 and 9 triangles is the same. Similarly the expansion that triangles 2 and 8 suffer is lees than the previous one and the same for the two triangles. Finally, the triangles 3 and 7 get compressed to the same extent. One additional observation is that the triangles are obviously not regular. These results complement the overall view of the chemisorption effects.

The local geometrical structure of the Au surface layer in the presence of the Mn atoms, for the fixed and intermediate state of the reaction path reported in Fig. 3, is shown in Fig. 5. This figure clearly shows how the surface geometrical structure undergoes local distortions as one of the Mn atom moves from the fixed position to the intermediate states (across the energy barriers). One observes that this modification is larger when the second Mn atom is located in the neighborhood of a bridge site.

### 3.4. Magnetocrystalline anisotropy energy

We studied the magnetocrystalline anisotropy energy (i.e.: due the spin–orbit coupling) of two selected arrangements (1–2) and (1–8). We observe that in both cases the easy axis is in-plane. In the (1–2) the anisotropy between an in-plane and out-of-plane orientation is 0.5 meV and the easy axis is along the Mn–Mn bond. In the case (1–8), this anisotropy is 1.9 meV, but the easy one is perpendicular to the Mn–Mn bond. Those energies are fairly large when compared to bulk anisotropies, but the 'sample' consists just of two atoms, and the system should be superparamagnetic at about 25 K.

### 3.5. The Shockley surface states

To get some insight of the role of the Au(111) Shockley state in the magnetic interaction, we simplified the system under study. First, to have a simpler picture, the $4 \times 4$ supercell was changed to a $1 \times 1$ and $2 \times 2$ supercell, in this way we avoid too many additional states due to down-folding. Next, even though, a slab with a thickness of 5 layers gives reasonable energies, it is well-known that to have a proper Shockley state, semi-infinite boundary conditions are necessary (e.g. by using Greens function based methods, such as KKR), but often a very large slab is sufficient. We found that a 48 layers thick slab (~11 nm) gives clear surfaces states, see Fig. 6. Even when the Au(111) surface states have a sizable Rashba splitting, we decided to ignore the spin–orbit coupling. This approximation is justified since the most important effect in the RKKY theory is to have two periods of oscillation (from the two $k_F$, one for each paraboloid), both periods are quite similar, and then the effect is only appreciable for very long Mn–Mn distances. Additionally the spin–orbit coupling raises about four times the computational cost and makes the analysis more difficult.

The Shockley states of a pristine Au(111) surface are shown in Fig. 6(a). These states are very well localized in the topmost layer (dark red points) – validating our slab approach – also there is a small contribution from inner sub-bands (pale yellow points). When the Au(111) surface is fully covered by a Mn layer, see Fig. 6 (b), the Au-derived Shockley states are spin-split (~0.25 eV) around $\bar{\Gamma}$. Also the Mn-*d* orbitals hybridize with Au-*s* states,

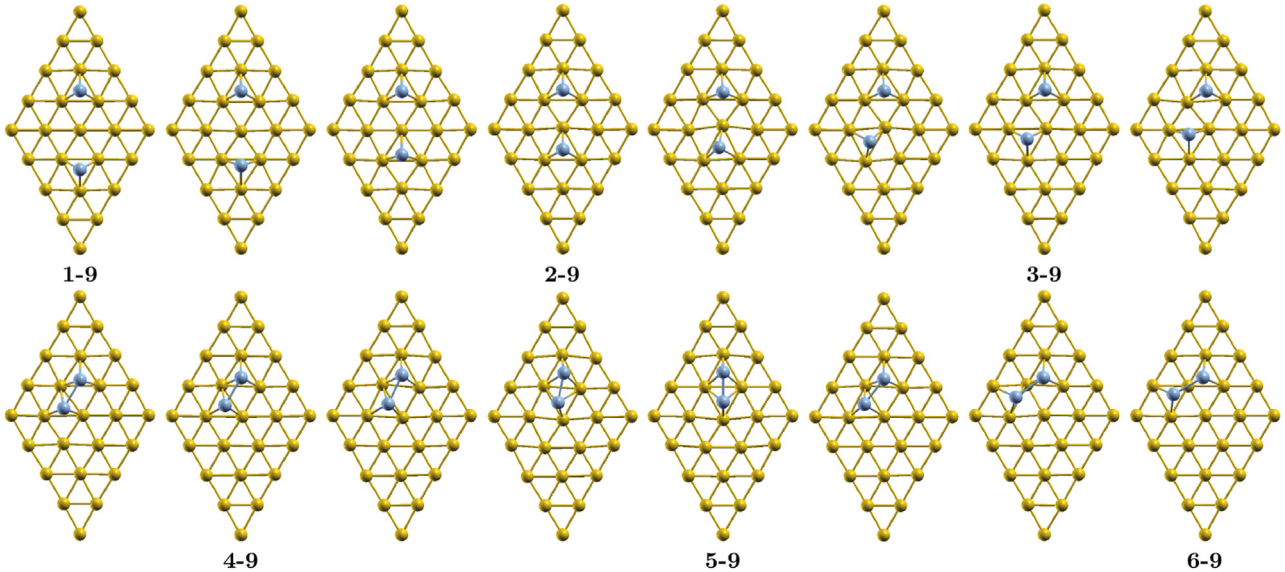


**Fig. 5.** Structures of the fixed (**1–9**, **2–9**, **3–9**, **4–9**, **5–9**, and **6–9** represented as blue triangles in Fig. 3) and some intermediate states of the energy barrier path calculated with the NEB method illustrated in Fig. 3. Gold and light blue atoms are for Au and Mn, respectively. (For interpretation of the references to color in this figure caption, the reader is referred to the web version of this paper.)

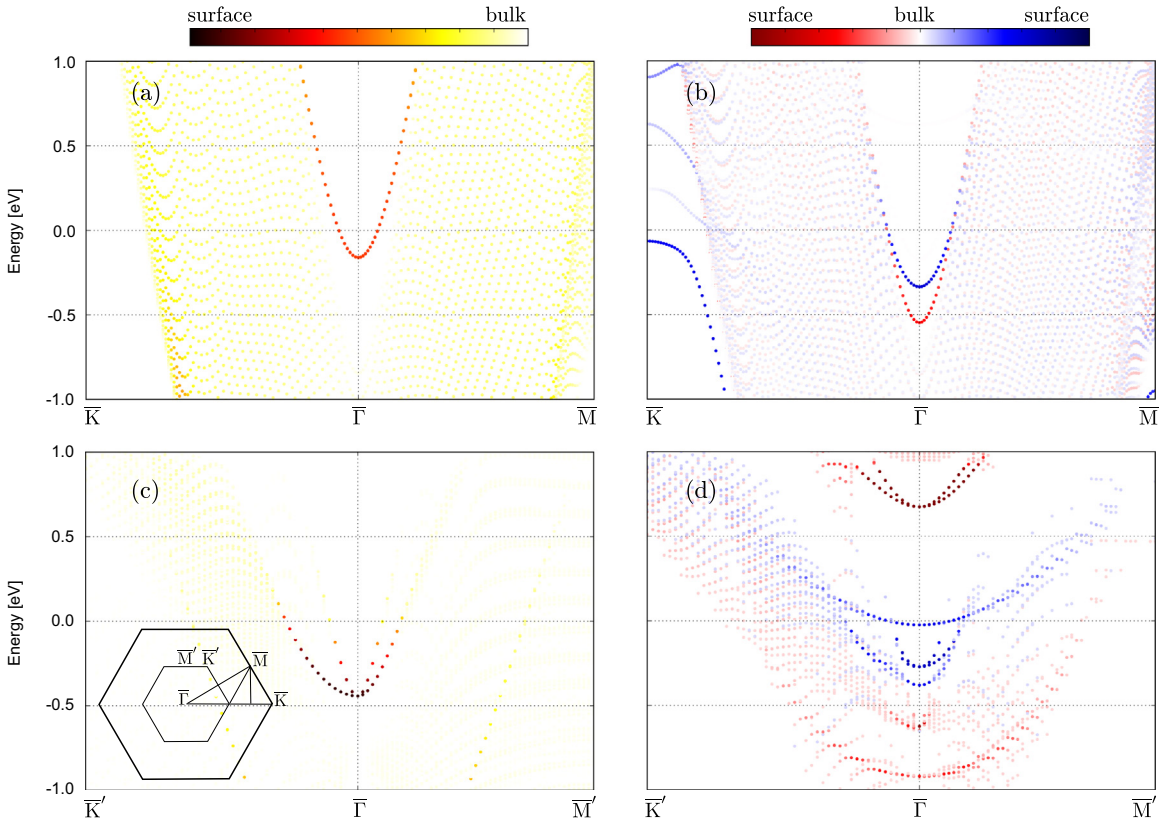


**Fig. 6.** Shockley states of (a) states of Au(111), (b) Au(111) when covered with Mn (coverage $\theta = 1$), (c) $2 \times 2$ Au(111) surface, and (d) $2 \times 2$ Au(111) surface covered with Mn $\theta = \frac{1}{4}$. The color scale shows the localization of the sub-bands (spin resolved when useful) on the desired surface. A scheme of the fundamental Brillouin zone, and its down-folding due the supercell is in panel (c). (For interpretation of the references to color in this figure caption, the reader is referred to the web version of this paper.)

producing some states at $\overline{\mathrm{K}}$. These states have a strong *d*-character far from $\overline{\mathrm{K}}$ and are localized close to the Mn layer (and then are omitted in the figure). The case of a full Mn monolayer also has dispersive, Mn-derived bands, which are not shown here for the sake of clarity.

To consider lower Mn coverages, it is needed to employ a supercell. We calculated a $2 \times 2$ Au(111) supercell with a Mn coverage of $\frac{1}{4}$. In this supercell the reciprocal vectors shrink to one half of their value in the primitive lateral cell. Both Brillouin zones, of the supercell and of the primitive cell, are sketched in Fig. 6(c), and also show how the irreducible Brillouin zone of the primitive cell folds to fit in the smaller Brillouin zone. Explicitly, the $\overline{\Gamma}$–$\overline{\mathrm{M}}$ line now is $\overline{\Gamma}$–$\overline{\mathrm{M}}$–$\overline{\Gamma}$ and $\overline{\Gamma}$–$\overline{\mathrm{K}}$ folds into $\overline{\Gamma}$–$\overline{\mathrm{K}}$–$\overline{\mathrm{M}}$–$\overline{\mathrm{K}}'$. Fig. 6(c) shows the surface states of a clean Au(111) surface, they are spin-degenerated, the additional states at $\overline{\Gamma}$ are due to band down-folding effects (even though they look like a sort of Rashba splitting, spin–orbit coupling is not included). Finally, the careful reader has noted that differences in the Fermi energy compared with the primitive lateral cell. This is just an artifact of using the clean side of a Mn-covered slab, the interaction with Mn (on the other side) lowers the Fermi energy, otherwise the physics remains unchanged.

When one Mn atom is deposited on the $2 \times 2$ surface, giving a coverage of $\frac{1}{4}$, the Au Shockley states are greatly affected, see Fig. 6 (d). The Au-*sp* surface state splits in three different states, as expected since the symmetry of the surface changes from $C_{3h}$ to $C_{1h}$; additionally, each band is strongly spin-split at $\overline{\Gamma}$. The Mn states (not shown) are practically dispersionless, indicating a small hybridization with the substrate.

From the previous results, we can conclude that when the Mn atoms are close – the case studied here – the coupling of the Mn atom to the Au substrate is due to the Au Shockley states. It could be in principle a RKKY interaction, but in practice, the potential describing the coupling and then the Shockley states are largely affected by Mn geometry. According to the RKKY theory [39], the period of the oscillations goes as the inverse of $k_F$, which is nearly 25 Å in the case of Au(111) [40]. This agrees with our study, since we found an AFM state up to a Mn–Mn distance of ~7 Å. The only exception is a small region between 3.1 and 3.9 Å. This region is a bridge site between two three-coordinated sites, giving us a hint that the FM state is linked with the geometry of the system. This is consistent with a reduction of the kinetic exchange (the hopping is affected by the geometry), due to the orthogonality of *p*-orbitals in the superexchange interaction (the Au(111) Shockley state is strongly *p* at $\overline{\Gamma}$). Then the interaction can be FM due to the remaining Coulomb exchange (i.e. a double-exchange mechanism).

### 3.6. STM images

Finally, we calculated the scanning tunneling microscopy (STM) images of the 1–2, 1–3, 1–4, 1–7, 1–8, and 1–9 geometries in the AF state. The top row of Fig. 7 shows the modeling of the STM images calculated within the Tersoff–Hamann approach [41] by using the partitioned charge density given by VASP. The images were generated at constant current (i.e. the tip of the microscope moves vertically up and down as it scans the surface), and the electronic densities were set to 0.1 $e$/Å$^3$. Similar values of electronic densities have been used in previous reports [20,21]. The states considered in the partitioned charge density are those in the zone 1 eV below the Fermi level.

The bottom row of Fig. 7 shows the isosurfaces of the charge density difference, $\Delta\rho(\mathbf{r})$, for the fixed AF states at an isovalue of 0.02 $e$/Å$^3$. Here $\Delta\rho(\mathbf{r})$ was calculated as follows:

$$\Delta\rho(\mathbf{r}) = \rho_T(\mathbf{r}) - \rho_s(\mathbf{r}) - \rho_{Mn}(\mathbf{r}), \quad (4)$$

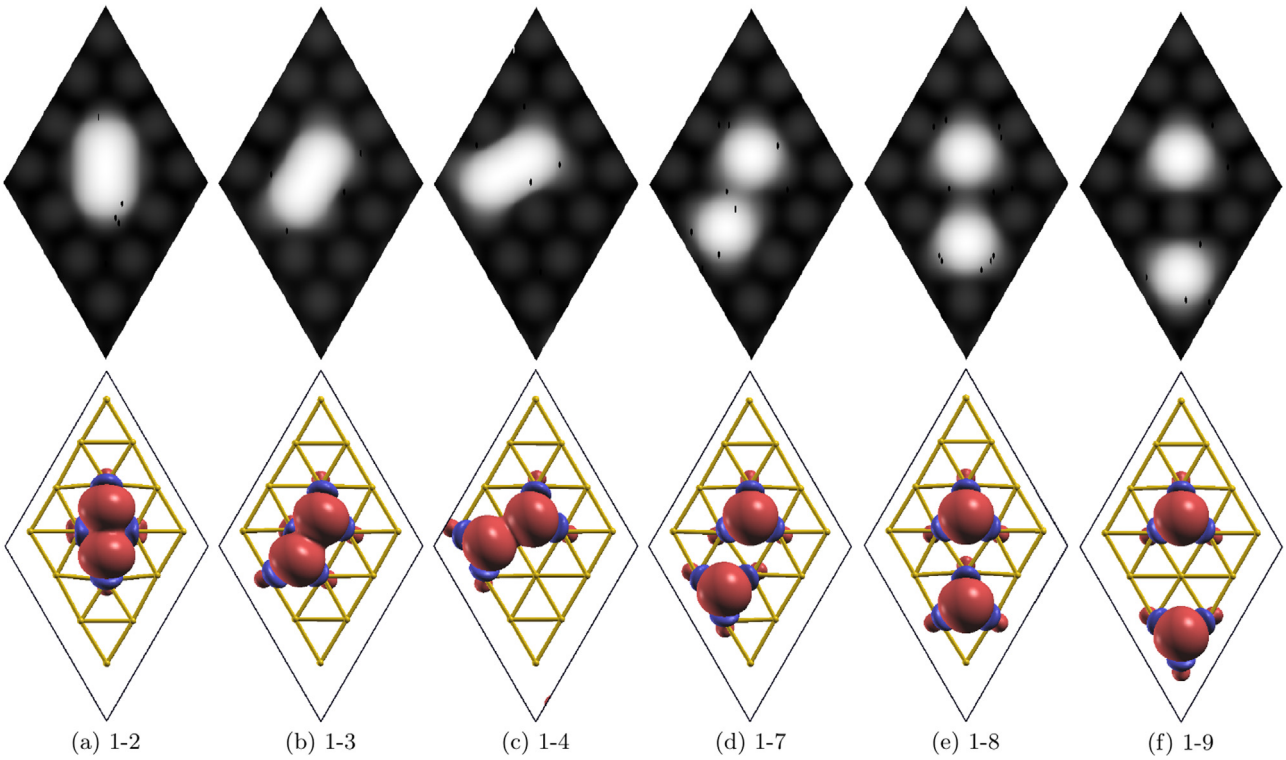


**Fig. 7.** Top row: STM images of a unit cell simulated for the 1–2, 1–3, 1–4, 1–7, 1–8, and 1–9 fixed AF states. Bottom row: isosurfaces of the difference charge densities for the fixed states: $\Delta\rho(\mathbf{r}) = \rho_T(\mathbf{r}) - \rho_S(\mathbf{r}) - \rho_{Mn}(\mathbf{r})$.

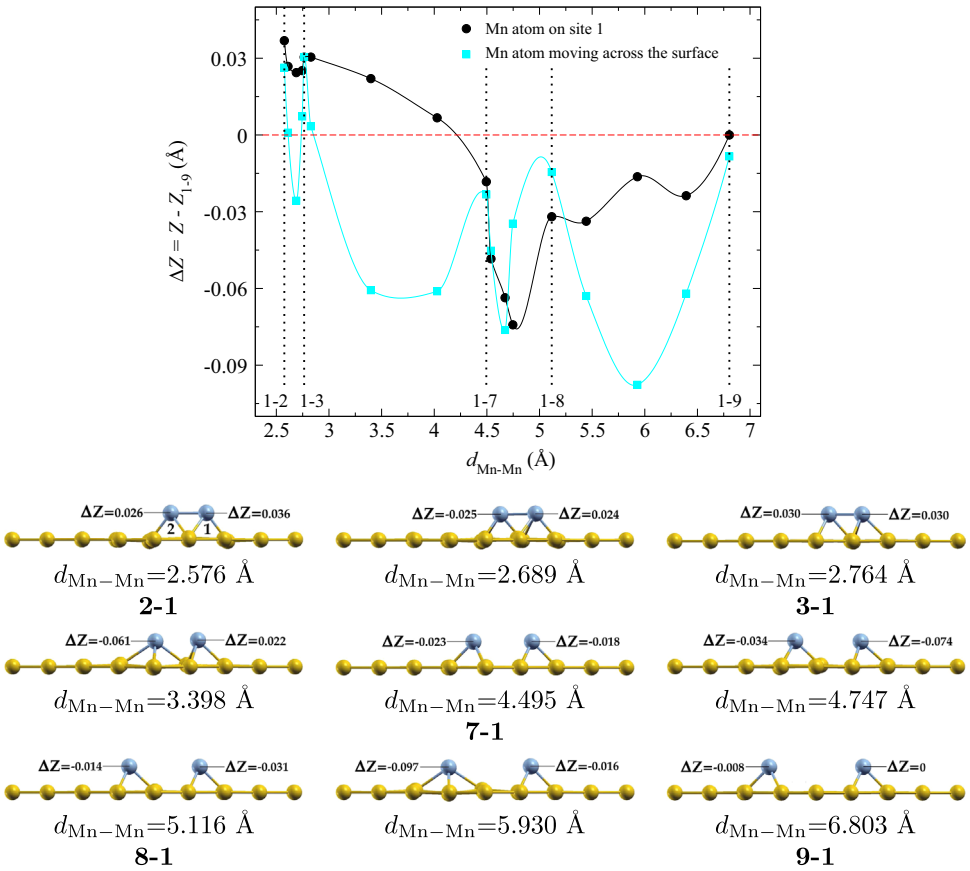


**Fig. 8.** Vertical displacement difference $\Delta Z$ of Mn atoms as a function of $d_{Mn-Mn}$ when Mn atom moves across the surface. Here $\Delta Z = Z - Z_{1-9}$, where $Z_{1-9}$ is the $Z$ distance for Mn atom adsorbed on site 1 when the other one is on site 9, i.e. 1–9 fixed site. Also, the structures for the fixed and some intermediate states with the corresponding $\Delta Z$ values (Å) are depicted.

where $\rho_T(\mathbf{r})$, $\rho_s(\mathbf{r})$, and $\rho_{Mn}(\mathbf{r})$ are the charge density from the optimized fixed state, the charge density of the fixed state without the Mn atoms, and the charge density of the Mn atoms at the positions of the fixed state, respectively. Although the densities of electrons close to the Fermi level are different in the ferro and antiferromagnetic states, it is not possible to discriminate the up from the down electrons and to draw conclusions related to the magnetic state. Nevertheless, the charge densities from bottom row of Fig. 7 show how the Mn atoms interact with the Au surface, which resemble the results from the simulated STM images.

To complement the information that may be used for STM experiments, we present in Fig. 8 the vertical displacement of the Mn atoms at site 1 $Z_{1,i}$ and the corresponding to the second atom $Z_{2,i}$ when we move the second atom from site $i=2$ to 9. We show also results for the intermediate points calculated with the NEB. Also, Fig. 8 shows some structures of the Au topmost layer with Mn atoms for the fixed and some intermediate states with the corresponding $\Delta Z$ values (Å). We take as the reference the $Z_{1,9}$ value of the Mn atom at site 1 when the second Mn atom is at site 9. It is important to note that the difference in $Z_{1,9}$ and $Z_{2,9}$ in those two far away sites is produced by the fact that one is of type fcc and the other hcp.

It is worth noticing that there are clear local minima for both atom displacements, $Z_{1,i}$ and $Z_{2,i}$ in Fig. 8, in the regions between 1–2 to 1–3, and 1–7 to 1–8. These cases correspond to the points where atom 2 crosses bridge geometries. Moreover, the AFM solution (presented in this figure) is not the most stable in region 1–3 to 1–7, see Section 3.2. One last observation is that the deformation that the Au triangles suffer when one Mn is located in the apex are almost the same when both sites correspond to fcc-sites (see Fig. 4). There is an expansion of the order of 12.5%.

## 4. Summary and conclusions

In summary, we have investigated part of landscape of the adsorption energies of a Mn dimer on Au(111) surface as a function of the interatomic bond distance among Mn atoms by means of the density functional theory. We show that the adsorption energy depends on the magnetic state as well as on the interatomic bond distance between the Mn atoms. Here we found three different behaviors: (i) the first, AFM from 2.58 to 3.10 Å, where the overall lowest energy state is at 2.765 Å, corresponding to next-nearest neighbor adsorption sites; (ii) a FM region from 3.10 to 3.91 Å; and (iii) a second AF zone, ranging from 3.91 to 6.8 Å. Our results are in relative well agreement with the previous study done in the free $Mn_2$ dimer, for which the magnetic coupling state of lower energy depends on the interatomic bond distance. In addition we have calculated the energy barriers that one of the two Mn atoms has to overcome when it moves across the surface. We show in detail how the surface geometry is perturbed upon the adsorption process, including an analysis of the Au Shockley state. Finally we modeled some scanning tunneling microscopy images, and showed calculated isosurfaces of the charge densities for some fixed states.

We hope that this study encourage experimental and theoretical researchers to investigate the interaction and diffusion of magnetic transition metal species like Mn on gold surfaces.

## Acknowledgements

The authors thank the support from CONACyT México under the program of CATEDRAS for young researchers (S.L.-M.), FONDECYT 11110510 (F.M.) and Financiamiento Basal para Centros Científicos y Tecnológicos de Excelencia (F.M. and J. M.-L.). FONDECYT Projects #1100365 (J.M-L.), 11110510 (F.M.) and 1150806 (F.M.) and Millennium Science Nucleus Project P10-061-F (J.M.-L.). We also acknowledged the computing time provided by Red Española de Supercomputación (RES) and MALTA-Cluster.

## References

[1] C. Demangeat, J. Parlebas, Electronic, magnetic and spectroscopic properties of manganese nanostructures, Rep. Prog. Phys. 65 (11) (2002) 1679, http://dx.doi.org/10.1007/978-3-642-04650-6_6.
[2] J. Mejía-López, A.H. Romero, M.E. Garcia, J.L. Morán-López, Noncollinear magnetism, spin frustration, and magnetic nanodomains in small $Mn_n$ clusters, Phys. Rev. B 74 (2006) 140405, http://dx.doi.org/10.1103/PhysRevB.74.140405.
[3] J. Mejía-López, A.H. Romero, M.E. Garcia, J.L. Morán-López, Understanding the elusive magnetic behavior of manganese clusters, Phys. Rev. B 78 (2008) 134405, http://dx.doi.org/10.1103/PhysRevB.78.134405.
[4] J.R. Lombardi, B. Davis, Periodic properties of force constants of small transition-metal and lanthanide clusters, Chem. Rev. 102 (2002) 2431–2460, http://dx.doi.org/10.1021/cr010425j.
[5] F. Heusler, Mangan-aluminium-kupferlegierungen, Verh. Dtsch. Phys. Ges. 5 (1903) 219.
[6] P. Webster, M. Ramadan, Magnetic order in palladium-based Heusler alloys Part I: $Pd_2MnIn_{1-x}Sn_x$ and $Pd_2MnSn_{1-x}Sb_x$, J. Magn. Magn. Mater. 5 (1) (1977) 51–59, http://dx.doi.org/10.1016/0304-8853(77)90196-2.
[7] A. Kant, S.-S. Lin, B. Strauss, Dissociation energy of $Mn_2$, J. Chem. Phys. 49 (4) (1968) 1983–1985, http://dx.doi.org/10.1063/1.1670350.
[8] T. Haslett, M. Moskovits, A. Weitzman, Dissociation energies of transition metal diatomics, J. Mol. Spectrosc. 135 (2) (1989) 259–269, http://dx.doi.org/10.1016/0022-2852(89)90155-0.
[9] A. Terasaki, T.M. Briere, M. Kulawik, S. Minemoto, K. Tono, A. Matsushita, T. Kondow, Ferromagnetic spin coupling in the manganese trimer ion evidenced by photodissociation spectroscopy, J. Chem. Phys. 118 (5) (2003) 2180–2185, http://dx.doi.org/10.1063/1.1534106.
[10] M. Cheeseman, R. Van Zee, W. Weltner Jr., Exchange striction in the $Mn_2$ molecule, J. Chem. Phys. 91 (4) (1989) 2748–2749, http://dx.doi.org/10.1063/1.456985.
[11] J.-C. Rivoal, J.S. Emampour, K.J. Zeringue, M. Vala, Ground-state exchange energy of the $Mn_2$ antiferromagnetic molecule, Chem. Phys. Lett. 92 (3) (1982) 313–316, http://dx.doi.org/10.1016/0009-2614(82)80283-2.
[12] K. Bier, T. Haslett, A. Kirkwood, M. Moskovits, The resonance raman and visible absorbance spectra of matrix isolated $Mn_2$ and $Mn_3$, J. Chem. Phys. 89 (1) (1988) 6–12, http://dx.doi.org/10.1063/1.455461.
[13] A. Kirkwood, K. Bier, J. Thompson, T. Haslett, A. Huber, M. Moskovits, Ultraviolet-visible and raman spectroscopy of diatomic manganese isolated in rare-gas matrixes, J. Phys. Chem. 95 (7) (1991) 2644–2652, http://dx.doi.org/10.1021/j100160a006.
[14] A.A. Buchachenko, G. Chałasiński, M.M. Szcześniak, Electronic structure and spin coupling of the manganese dimer: the state of the art of *ab initio* approach, J. Chem. Phys. 132 (2) (2010) 024312, http://dx.doi.org/10.1063/1.3292572.
[15] M. Fonin, Y.S. Dedkov, U. Rüdiger, G. Güntherodt, Growth and structure of Mn on Au(111) at room temperature, Surf. Sci. 529 (3) (2003) L275–L280, http://dx.doi.org/10.1016/S0039-6028(03)00272-3.
[16] O. Rader, W. Gudat, C. Carbone, E. Vescovo, S. Blügel, R. Kläsges, W. Eberhardt, M. Wuttig, J. Redinger, F.J. Himpsel, Electronic structure of two-dimensional magnetic alloys: $c(2\times2)$ Mn on Cu(100) and Ni(100), Phys. Rev. B 55 (1997) 5404–5415, http://dx.doi.org/10.1103/PhysRevB.55.5404.
[17] C. Ross, B. Schirmer, M. Wuttig, Y. Gauthier, G. Bihlmayer, S. Blügel, Structure, growth, and magnetism of Mn on Cu(110), Phys. Rev. B 57 (1998) 2607–2620, http://dx.doi.org/10.1103/PhysRevB.57.2607.
[18] P. Schieffer, C. Krembel, M.-C. Hanf, G. Gewinner, Y. Gauthier, Evidence of $c(2\times2)$ antiferromagnetic order of Mn in an ideal monolayer on Ag(001), Phys. Rev. B 62 (2000) 2944–2955, http://dx.doi.org/10.1103/PhysRevB.62.2944.
[19] T. Sachse, N. Néel, S. Meierott, R. Berndt, W. Hofer, J. Kröger, Electronic and magnetic states of $Mn_2$ and $Mn_2H$ on Ag(111), New J. Phys. 16 (6) (2014) 063021, http://dx.doi.org/10.1088/1367-2630/16/6/063021.
[20] F. Muñoz, A.H. Romero, J. Mejía-López, J.L. Morán-López, Monoatomic and dimer Mn adsorption on the Au(111) surface from first principles, Phys. Rev. B 83 (2011) 205423, http://dx.doi.org/10.1103/PhysRevB.83.205423.
[21] F. Muñoz, A.H. Romero, J. Mejía-López, J.L. Morán-López, First-principles theoretical investigation of monoatomic and dimer Mn adsorption on noble metal (111) surfaces, Phys. Rev. B 85 (2012) 115417, http://dx.doi.org/10.1103/PhysRevB.85.115417.
[22] P.E. Blöchl, Projector augmented-wave method, Phys. Rev. B 50 (1994) 17953–17979, http://dx.doi.org/10.1103/PhysRevB.50.17953.
[23] G. Kresse, D. Joubert, From ultrasoft pseudopotentials to the projector augmented-wave method, Phys. Rev. B 59 (1999) 1758–1775, http://dx.doi.org/10.1103/PhysRevB.59.1758.
[24] G. Kresse, J. Hafner, *Ab initio* molecular dynamics for liquid metals, Phys. Rev. B 47 (1993) 558–561, http://dx.doi.org/10.1103/PhysRevB.47.558.

[25] G. Kresse, J. Hafner, *Ab initio* molecular-dynamics simulation of the liquid-metal amorphous-semiconductor transition in germanium, Phys. Rev. B 49 (1994) 14251–14269, http://dx.doi.org/10.1103/PhysRevB.49.14251.
[26] G. Kresse, J. Furthmüller, Efficiency of *ab-initio* total energy calculations for metals and semiconductors using a plane-wave basis set, Comput. Mat. Sci. 6 (1996) 15, http://dx.doi.org/10.1016/0927-0256(96)00008-0.
[27] G. Kresse, J. Furthmüller, Efficient iterative schemes for *ab initio* total-energy calculations using a plane-wave basis set, Phys. Rev. B 54 (1996) 11169–11186, http://dx.doi.org/10.1103/PhysRevB.54.11169.
[28] J.P. Perdew, K. Burke, M. Ernzerhof, Generalized gradient approximation made simple, Phys. Rev. Lett. 77 (1996) 3865–3868, http://dx.doi.org/10.1103/PhysRevLett.77.3865.
[29] C. Kittel, Introduction to Solid State Physics, seventh ed., John Wiley & Sons, London, 1996.
[30] F. Hanke, J. Björk, Structure and local reactivity of the Au(111) surface reconstruction, Phys. Rev. B 87 (2013) 235422, http://dx.doi.org/10.1103/PhysRevB.87.235422.
[31] S.A. Lindgren, L. Walldén, J. Rundgren, P. Westrin, Low-energy electron diffraction from Cu(111): subthreshold effect and energy-dependent inner potential; surface relaxation and metric distances between spectra, Phys. Rev. B 29 (1984) 576–588, http://dx.doi.org/10.1103/PhysRevB.29.576.
[32] H.J. Monkhorst, J.D. Pack, Special points for Brillouin-zone integrations, Phys. Rev. B 13 (1976) 5188–5192, http://dx.doi.org/10.1103/PhysRevB.13.5188.
[33] J. Wan, Y.L. Fan, D.W. Gong, S.G. Shen, X.Q. Fan, Surface relaxation and stress of fcc metals: Cu, Ag, Au, Ni, Pd, Pt, Al and Pb, Model. Simul. Mater. Sci. Eng. 7 (2) (1999) 189, http://dx.doi.org/10.1088/0965-0393/7/2/005.
[34] S.M. Foiles, M.I. Baskes, M.S. Daw, Embedded-atom-method functions for the fcc metals Cu, Ag, Au, Ni, Pd, Pt, and their alloys, Phys. Rev. B 33 (1986) 7983–7991, http://dx.doi.org/10.1103/PhysRevB.33.7983.
[35] V. Zólyomi, L. Vitos, S.K. Kwon, J. Kollár, Surface relaxation and stress for 5*d* transition metals, J. Phys.: Condens. Matter 21 (9) (2009) 095007, http://dx.doi.org/10.1088/0953-8984/21/9/095007.
[36] S. López-Moreno, A.H. Romero, Atomic and molecular oxygen adsorbed on (111) transition metal surfaces: Cu and Ni, J. Chem. Phys. 142 (15) (2015) 154702, http://dx.doi.org/10.1063/1.4917259.
[37] H. Jónssoni, G. Mills, K.W. Jacobsen, Nudged Elastic Band Method for Finding Minimum Energy Paths of Transitions, World Scientific, Singapore (1998), pp. 385–404 (chapter 16).
[38] G. Henkelman, G. Jóhannesson, H. Jónsson, Methods for Finding Saddle Points and Minimum Energy Paths, Kluwer Academic, New York (2000), pp. 269–300 (chapter 10).
[39] K. Yosida, Magnetic properties of Cu–Mn alloys, Phys. Rev. 106 (5) (1957) 893, http://dx.doi.org/10.1103/PhysRev.106.893.
[40] E. Simon, B. Újfalussy, B. Lazarovits, A. Szilva, L. Szunyogh, G.M. Stocks, Exchange interaction between magnetic adatoms on surfaces of noble metals, Phys. Rev. B 83 (22) (2011) 224416, http://dx.doi.org/10.1103/PhysRevB.83.224416.
[41] J. Tersoff, D.R. Hamann, Theory of the scanning tunneling microscope, Phys. Rev. B 31 (1985) 805–813, http://dx.doi.org/10.1103/PhysRevB.31.805.